Title
Protruded retinal layers within the optic nerve head neuroretinal rim

Journal
Acta Ophthalmologica, 96(4)

ISSN
1755-375X

Authors
Torres, Lucas A
Vianna, Jayme R
Jarrar, Faisal
et al.

Publication Date
2018-06-01

DOI
10.1111/aos.13657

Peer reviewed

HHS Public Access

Author manuscript

Acta Ophthalmol. Author manuscript; available in PMC 2019 June 01.

Published in final edited form as:

Acta Ophthalmol. 2018 June ; 96(4): e493–e502. doi:10.1111/aos.13657.

Protruded Retinal Layers Within the Optic Nerve Head Neuroretinal Rim

Lucas A. Torres[1], **Jayme R. Vianna**[1], **Faisal Jarrar**[1], **Glen P. Sharpe**[1], **Makoto Araie**[2], **Joseph Caprioli**[3], **Shaban Demirel**[4], **Christopher A. Girkin**[5], **Masanori Hangai**[6], **Aiko Iwase**[7], **Jeffrey M. Liebmann**[8,*], **Christian Y. Mardin**[9], **Toru Nakazawa**[10], **Harry A. Quigley**[11], **Alexander F. Scheuerle**[12], **Kazuhisa Sugiyama**[13], **Hidenobu Tanihara**[14], **Goji Tomita**[15], **Yasuo Yanagi**[16,*], **Claude F. Burgoyne**[4], and **Balwantray C. Chauhan**[1]

[1]Department of Ophthalmology and Visual Sciences, Dalhousie University, Halifax, NS, Canada

[2]Kanto Central Hospital of the Mutual Aid Association of Public School Teachers, Tokyo, Japan

[3]Department of Ophthalmology, Jules Stein Eye Institute, University of California Los Angeles, Los Angeles, CA

[4]Devers Eye Institute, Legacy Research Institute, Portland, OR

[5]Department of Ophthalmology, University of Alabama at Birmingham, Birmingham, AB

[6]Department of Ophthalmology, Saitama Medical School, Moro, Japan

[7]Tajimi Iwase Eye Clinic, Tajimi, Japan

[8]New York Eye and Ear Infirmary, New York University School of Medicine, New York, NY

[9]Department of Ophthalmology, University of Erlangen, Erlangen, Germany

[10]Department of Ophthalmology, Tohoku University Graduate School of Medicine, Tohoku, Japan

[11]Wilmer Ophthalmological Institute, Johns Hopkins University, Baltimore, MD

[12]Department of Ophthalmology, University of Heidelberg, Heidelberg, Germany

[13]Department of Ophthalmology and Visual Science, Kanazawa University Graduate School of Medical Science, Kanazawa, Japan

[14]Department of Ophthalmology, Faculty of Life Sciences, Kumamoto University, Kumamoto, Japan

[15]Department of Ophthalmology, Toho University Ohashi Medical Center, Tokyo, Japan

[16]Department of Ophthalmology, The University of Tokyo Graduate School of Medicine, Tokyo, Japan

Corresponding Author: Balwantray C. Chauhan, PhD, Department of Ophthalmology and Visual Sciences, Dalhousie University, 1276 South Park Street, 2W Victoria, Room 2035, Halifax, NS, Canada B3H 2Y9, Tel: (902) 473-3202; Fax: (902) 473-2839; bal@dal.ca.

*Current affiliations: Bernard and Shirlee Brown Glaucoma Research Laboratory, Edward S. Harkness Eye Institute, Columbia University Medical Center, New York, NY (JML); Singapore Eye Research Institute, Singapore National Eye Centre, Singapore (YY)

DR. LUCAS A. TORRES (Orcid ID : 0000-0003-4136-7362)

DR. TORU NAKAZAWA (Orcid ID : 0000-0002-5591-4155)

DR. BALWANTRAY CHAUHAN (Orcid ID : 0000-0002-7936-6907)

Abstract

Purpose—To determine the frequency with which retinal tissues other than the nerve fibre layer, hereafter referred to as protruded retinal layers (PRL), are a component of optical coherence tomography (OCT) neuroretinal rim measurements.

Methods—Ninety healthy (30 White, Black and Japanese, respectively) subjects were included in the study. A radial scan pattern (24 B-scans centred on Bruch's membrane opening [BMO]) was used. For each of the 48 minimum rim width (MRW) measurement points, we determined whether PRL were present, absent or indeterminate. When present, the proportion of PRL within the MRW was quantified.

Results—PRL were present in 503 (11.6%), absent in 3805 (88.1%) and indeterminate in 12 (0.3%) measurement points. Overall, 69 (76.6%) subjects had ≥1 points with PRL, with White subjects having the highest frequency and Japanese the lowest (29 [97%] and 18 [60%], respectively; $P < 0.01$). PRL were present in one-third of points in the temporal sector, but ≤ 5% in other sectors. When present, the median PRL thickness was 53.0 (interquartile range [IQR]: 33.0 to 78.5) μm, representing 20.6 (IQR: 13.0 to 28.5)% of MRW. Globally, the median PRL thickness comprised 1.3 (IQR: 0.2 to 3.5)% of the MRW, however, in the temporal sector, it exceeded 30% of MRW in some subjects.

Conclusions—PRL are a component of MRW measurements in most normal subjects, occurring in almost 12% of all measurement points analyzed. There were racial variations in the presence of PRL and a significantly higher frequency of PRL in the temporal sector.

Introduction

Advances in optical coherence tomography (OCT) have allowed a detailed appraisal of optic nerve head anatomy, leading to new concepts for the acquisition, analysis and interpretation of OCT data. For example, OCT has revealed that the clinically visible optic disc margin is not a consistent anatomical structure from which the neuroretinal rim can be assessed (Chauhan & Burgoyne 2013, Reis et al. 2012, Strouthidis et al. 2009). Many investigators have now proposed that Bruch's membrane opening (BMO), which is readily identified with OCT, but not always with funduscopic examination, is a consistent outer border of the rim that should be used as a reference point for its measurement (Reis et al. 2012, Strouthidis et al. 2009, Strouthidis et al. 2009). Furthermore, unlike classical rim measurements, which are made in the fixed plane of the disc margin, newer research supports measurement of the minimum width from BMO to the internal limiting membrane. This parameter is termed minimum rim width (MRW), and allows the direction, or MRW vector, to vary according to the orientation of the rim tissue (Chen 2009, Gardiner et al. 2014, Povazay et al. 2007, Reis et al. 2012, Strouthidis et al. 2011). These new principles have led to increased diagnostic accuracy for glaucoma (Chauhan et al. 2013) and a better alignment of these structural parameters to visual field findings (Danthurebandara et al. 2014, Pollet-Villard et al. 2014).

In addition to axons of retinal ganglion cells, the neuroretinal rim contains other elements, such as blood vessels and glial tissue (Varela & Hernandez 1997, Wang et al. 2002), likely contributing to the sub-optimal relationship between rim measurements and the visual field, or even retinal nerve fibre layer (RNFL) thickness. While this sub-optimal relationship is

perceived to problematic, it is also reasonable to propose that identifying the non-axonal components of the rim may improve our understanding of their behaviour in glaucoma.

Fortune and colleagues (Fortune et al. 2016) recently reported in monkeys that MRW measurements could contain not just the RNFL, but portions of the outer and middle retinal layers. Indeed, they argued that the presence of these 'protruded' retinal layers in the rim measurement could be another reason why the observed correlation between MRW and actual axonal counts in monkey was not as strong as the correlation between RNFL thickness and axon counts.

To determine the potential importance of protruded retinal layers (PRL) in humans, we performed this study to assess their frequency and magnitude within the MRW of healthy subjects. As previous studies with OCT showed variation in optic nerve head (ONH) anatomy, for example in cup-disc ratio (Knight et al. 2012), optic disc area (Girkin et al. 2011, Knight et al. 2012), and laminar depth (Rhodes et al. 2014), according to different races, we report data in White, Black and Japanese normal subjects. We also investigated whether orientation of the border tissue of Elschnig (Anderson & Hoyt 1969) had an influence on the presence and extent of PRL in MRW measurements.

Methods

Participants

Data were acquired from a larger series of multi-centre studies characterising the ONH, RNFL and macula in normal subjects. The subjects in this report comprised a sub-sample of 30 individuals each in three groups that self-identified as White, Black or Japanese. Each participating institution received approval from its Ethics Review Board. In accordance with the Declaration of Helsinki, all participants provided informed consent.

Subjects were included if all the following criteria were met: (1) normal eye examination without vitreoretinal or choroidal disease or prior intraocular surgery (except cataract or refractive surgery), (2) intraocular pressure of 21 mmHg or less, (3) best-corrected visual acuity of 20/40 or better, (4) refractive spherical error within 6 diopter (D) and cylinder error within 2D, and (5) normal visual field, defined by a normal glaucoma hemifield test and mean deviation within normal limits. Subjects were excluded if either of the following were found: (1) unreliable visual field examination results based on the reliability indices and the perimetrist's notes, or (2) OCT images of insufficient quality (truncated B-scans where the internal limiting membrane could not be segmented and/or image quality score < 20). When both eyes were eligible, only one randomly selected eye was used for the analysis.

The 30 subjects per race group were determined as follows. We first computed the maximum number of subjects that would allow the same sample size for each race in each of the 6 decade groups. To maintain the same number of subjects per decade group and race, the sample size was dictated by the minimum number of subjects in each decade group, which in this case was 5 (among those aged 70–80 years). We then randomly selected 5 subjects per race in each of the other decade groups.

OCT Imaging

The ONH was imaged with OCT (Spectralis; Heidelberg Engineering GmbH, Heidelberg, Germany) with software version VV (Heyex, Heidelberg Engineering). The scan pattern consisted of 24 radially equidistant B-scans, each subtending 15°, and was aligned and acquired according to the subject's own fovea-to-BMO centre axis (Chauhan et al. 2015). Each B-scan contained 768 A-scans and was derived from an average of 25 individual scans. Each B-scan contained 2 BMO points (180° apart), hence there were 2 MRW measurements per scan and 48 per eye. At each measurement point, the MRW angle represented the angle between the MRW plane of measurement and the BMO reference line, which connects the two BMO points of each scan.

Image segmentation

At each MRW measurement point, PRL, defined as any retinal layer besides the RNFL included within the MRW based on layer contrast in unenhanced B-scans (Fig. 1), were classified as being present, absent or indeterminate. The latter category occurred typically when there were shadows cast by overlying blood vessels at the point of measurement or when it was uncertain whether outer retinal layers were or were not within the MRW. When PRL were present, their width was measured with the calliper tool of the software along the MRW vector (Fig. 1).

Border tissue obliqueness (Reis et al. 2012, Strouthidis et al. 2009, Strouthidis et al. 2009) was measured for each of the two measurement points within each B-scan. A straight line that best approximated the border tissue and scleral canal was drawn first, starting at BMO. Next, a reference line connecting the two BMO points was determined. The angle between the border tissue plane and the BMO reference line was defined as border tissue angle (Vianna et al. 2016), with internally oblique border tissue (Reis et al. 2012, Strouthidis et al. 2009, Strouthidis et al. 2009) configurations having an angle greater than 90° and externally oblique (Reis et al. 2012, Strouthidis et al. 2009, Strouthidis et al. 2009) configurations having an angle less than 90° (Fig. 2). The orientation of the MRW vector relative to the BMO reference plane was also computed at each MRW measurement point and defined as MRW angle, with MRW angle increasing as the MRW vector was oriented further from BMO centre (Fig. 3).

Image segmentation for the first 12 (13%) subjects was performed together by 3 examiners (LT, FJ and BCC) to discuss and ensure agreement on how to judge and segment the images. Thereafter, a single examiner (FJ) segmented the images for all remaining 78 (87%) subjects. All image segmentations were then reviewed by two examiners (LT and FJ) and corrected when necessary.

Reproducibility of image segmentations

The intra-individual agreement for assessing the presence and extent of PRL as well as in the assessment of border tissue angle was determined for one observer (FJ), who segmented most of the images. OCT images were obtained in the same manner as described above for an independent group of 15 White healthy subjects, which were used to perform the reproducibility analysis. The examiner segmented the OCT images twice, on different days.

Statistical analysis

Data were summarised with median and interquartile range (IQR) values. Comparisons of continuous variables among the three races were performed with the Kruskal-Wallis test, while the comparisons of categorical values utilized the chi-squared test. Kappa statistics were used for the reproducibility study.

The number of MRW measurement points with PRL was calculated globally and in each of 6 ONH sectors as described previously (Garway-Heath et al. 2000). From the 48 points evaluated in each subject, 15 were located in the nasal sector, 13 in the temporal and 5 in each of the others sectors (supero-nasal, supero-temporal, infero-nasal and infero-temporal).

For each measurement point in which PRL were present, an adjusted MRW was calculated by subtracting the PRL thickness from the total or unadjusted MRW. The global unadjusted and adjusted MRW were calculated as averages for each subject. For this calculation, measurement points where the presence of PRL was classified as absent or indeterminate were given a PRL thickness value of 0.0 μm.

Linear regression was used to estimate the correlation between BMO area and the number of MRW measurement points with PRL per eye. The influence of border tissue angle at each point on the presence of PRL was evaluated with a mixed-effects logistic model. Mixed effect models were used to account for the correlation between multiple observations (i.e., measurement points) from each subject. Data analysis was performed with the open-source software R (version 3.3.1), and package lmer4 (version 1.1–12).

Results

Key characteristics of the study subjects are shown in Table 1. There were some differences among the groups: Black subjects were the most myopic; Japanese subjects had the largest BMO area and the thinnest global unadjusted MRW (all $P < 0.01$).

In the reproducibility study, the kappa statistic for intra-individual agreement for categorising the presence or absence of PRL was 0.82, classified as ‘almost perfect’ according to Landis and Koch (Landis & Koch 1977). The median difference between the two evaluations of PRL thickness was 0 (IQR: −12 to 4.5) μm, while the corresponding figure for border tissue angle was 0.1 (IQR: −5.8 to 5.0) °.

With 24 B-scans (48 MRW measurement points) per subject, there were a total of 4320 points analyzed. PRL were present in 503 (11.6%) points, absent in 3805 (88.1%) and labeled as indeterminate in 12 (0.3%) points. Overall, 69 (76.6%) subjects had ≥1 points with PRL within MRW (Table 2): the frequency was highest in White subjects (29 [97%]), then Black subjects (22 [73%]) and lowest in Japanese subjects (18 [60%]). The temporal sector had the highest number of MRW measurement points with PRL: 391 (33.4%) of 1170 points; while the frequencies in the other sectors were: 13 (2.8%) of 450 points in the infero-temporal sector, 23 (5.1%) of 450 in the supero-temporal sector, 64 (4.7%) of 1350 in the nasal sector, 6 (1.3%) of 450 in the infero-nasal sector and 6 (1.3%) out of 450 in the supero-nasal sector (Fig. 4).

For the measurement points in which PRL were present, the median PRL thickness and PRL thickness, relative to unadjusted MRW, was 53.0 (IQR: 33.0 to 78.5) μm and 20.6 (IQR: 13.0 to 28.5)%, respectively (Fig. 5). The global and sectoral distributions of PRL thickness and the PRL thickness relative to unadjusted MRW are shown in Figure 6. Globally, the median PRL thickness was 4.1 (IQR: 0.5 to 10.3) μm, comprising 1.3 (IQR: 0.2 to 3.5)% of the unadjusted MRW. The temporal sector had the largest median PRL thickness with a median of 13.0 (IQR: 0.0 to 30.1) μm, comprising 5.5 (IQR: 0.0 to 13.7)% of the unadjusted MRW. In the other sectors, the median PRL thickness was 0.0 μm (Fig. 6).

The median MRW angle nasally was close to 90°, indicating a close to vertical MRW vector compared to temporally, superiorly or inferiorly, which had a more horizontal MRW vector towards to the BMO centre (Figs. 3 and 7). In measurement points with PRL, the corresponding MRW angle was generally greater than the median for all points, indicating a MRW vector more external to the BMO centre (Fig. 7).

The lowest values of border tissue angle, indicating more externally oblique border tissue configuration, occurred in the temporal and infero-temporal sectors, while the highest values, indicating more internally oblique border tissue configuration, occurred more frequently in the nasal and supero-nasal sectors (Fig. 8). There was a negative association between the proportion of measurement points with PRL and border tissue angle (odds ratio for frequency of PRL = 0.84 (CI: 0.82 - 0.87) for each 10° of increase in border tissue angle, $P < 0.01$; Fig. 9) indicating that there was a lesser likelihood of PRL with increasingly internally oblique border tissue angle. The proportion of MRW measurement points with PRL was particularly high in extreme externally oblique border tissue configurations (angles ≤ 30°). There was a poor relationship between BMO area and the number of measurement points with PRL (adjusted $R^2 = 0.00$, $P = 0.68$; Fig. 10).

Discussion

Fortune et al (Fortune et al. 2016) previously identified PRL in OCT images of monkey ONHs and speculated that the PRL could be one of the reasons for the weaker correlation between rim parameters and axons counts compared to that between peripapillary RNFL thickness and axons counts. In the present study we assessed the frequency with which PRL were detected within the neuroretinal rim and the impact they had on MRW measurements in a multiracial sample of healthy subjects. PRL were identified in at least one B-scan in 69 (76.6%) subjects and in 503 (11.6%) MRW measurement points examined, over one-third of which were in the temporal sector. When present, the median PRL thickness in the temporal sector was 53 μm, corresponding to 20.6% of the unadjusted MRW. In the temporal sector, the PRL thickness made up 5.5% of the unadjusted MRW, however, in some subjects this proportion exceeded 30% (Fig. 6). Globally, PRL accounted for 1.3% of the MRW and in no subject did it exceed 10%.

Although OCT is now a well-established tool to help clinicians assess structural glaucomatous damage with objective measurements of the ONH rim, peripapillary RNFL and the macular ganglion cell layer, there are potential limitations of these parameters and questions regarding what precisely they measure. If the goal of these parameters is to relate

to retinal ganglion cell function, then they should specifically provide an estimate of functional ganglion cell components, and not include non-neural components such as blood vessels, connective or glial tissue. Current technology does not allow subtraction of all non-neural components from the width, area or volume measurements currently in use, however, attempts to account for blood vessels, suggested by some authors (Knighton et al. 2012, Patel et al. 2014, Ye et al. 2016) to adjust rim measurements for the PRL could help in this regard. However, it is important to recognize that also glaucoma affects non-neural tissues also (Yang et al. 2015, Yang et al. 2017, Yang et al. 2011) and that while the inclusion of these components may result in a less than perfect alignment with functional loss, it does not mean that diagnostic accuracy for glaucoma is adversely affected.

In addition to documenting the frequency of PRL and its magnitude within the neuroretinal rim, we also addressed factors related to the presence of PRL. Although our study was limited by a relatively small sample size, we found a consistent difference in PRL frequency among races, with the Japanese having the lowest frequency. Racial differences among structural measurements have already been shown in parameters of the ONH, for example, in the cup-disc ratio (Knight et al. 2012), optic disc area (Girkin et al. 2011, Knight et al. 2012), laminar depth (Rhodes et al. 2014) and BMO area (Rhodes et al. 2015, Rhodes et al. 2017). The clinical relevance of these inter-racial differences in ONH parameters are still not clear (Knight et al. 2012, Rao et al. 2010, Zelefsky et al. 2006). Although race-specific normative databases may be an alternative to deal with these differences (Zelefsky et al. 2006), the large within-race variability of these parameters indicates there would be little benefit of accounting for race in diagnostic tests for glaucoma (Rhodes et al. 2017). The MRW adjustment for PRL thickness would lead to a smaller inter-racial difference of MRW, as White and Black subjects, who had thicker MRW, also had a higher frequency of PRL compared to Japanese subjects, in whom the BMO area was largest. Therefore, even if future studies demonstrated that adjusting MRW for PRL thickness is clinically beneficial, it will be unlikely that specific normative databases for each race would be necessary.

We observed that PRL were more frequently found in the temporal sector, where there also was a higher likelihood of the border tissues having an externally oblique configuration. In our study we assumed that the border tissues and the anterior scleral canal were continuous to define neural canal obliqueness, however, this assumption may not be valid, as we did not separately segment these two structures. Nonetheless how border tissue or neural canal obliqueness could influence the presence of PRL is not clear. We also showed that the presence of PRL was related to the orientation of MRW: most points with PRL had a MRW vector that was oriented further from the BMO centre than the corresponding one for the entire population. However, it is interesting to note that although nasal points had a higher median MRW angle compared to temporal points (indicating that MRW was oriented more externally relative to the BMO centre), it was rare to observe PRL nasally compared to temporally where PRL were more frequently present. This observation suggests that the retinal layers protruding within the rim might be closer to BMO temporally compared to nasally. The higher density of photoreceptors (Curcio et al. 1990) and retinal ganglion cells (Curcio & Allen 1990) temporal to the ONH and the centrifugal displacement of the inner retinal layers at the fovea (Springer & Hendrickson 2004, Springer & Hendrickson 2004,

Springer & Hendrickson 2005) support our findings, though we did not measure the proximity of the retinal layers to BMO.

Because our study included only healthy subjects, we cannot yet speculate on the clinical implications of our findings. How glaucoma disease severity influences the presence of PRL and the clinical implications of these findings require additional studies, now in progress, that are beyond the scope of this report. The differences in the frequency, magnitude and especially sectoral variation in the presence of PRL among healthy subjects may suggest that adjusting MRW for PRL thickness could impact diagnostic accuracy.

There is considerable controversy in the literature as to whether retinal layers distal to the inner plexiform layer are affected in glaucoma. Histological studies in both experimental monkey glaucoma and human glaucoma eyes indicate either modest (Fan et al. 2011, Lei et al. 2008, Werner et al. 2011, Wygnanski et al. 1995) or no (Hasegawa et al. 2016, Ishikawa et al. 2005, Kendell et al. 1995, Kotowski et al. 2012) photoreceptor layer loss. Retinal ganglion cells have their somas in the ganglion cell layer, their axons in the RNFL and their dendrites in the inner plexiform layer. Thus it is expected that in addition to the RNFL loss, there is thinning of the ganglion cell layer (Ishikawa et al. 2005, Na et al. 2012, Tan et al. 2008, Wilsey et al. 2016), and the inner plexiform layer (Wilsey et al. 2016) in glaucoma that is readily detectable with OCT. We did not perform manual segmentation of each retinal layer (except the RNFL) within the PRL and therefore cannot speculate whether, in single examinations, potential damage to the other retinal layers in glaucoma could impact diagnostic accuracy of MRW. If there were no progressive loss of the outer retina in glaucoma, the presence of PRL would not be expected to impact the value of MRW for monitoring serial changes in the neuroretinal rim. In a possible scenario of progressive PRL thinning, the rate of MRW change would be amplified by the inclusion of PRL in the MRW measurements.

In the present study, one-third of the MRW measurement points in the temporal sector had PRL. This finding may be one of several reasons to explain why the temporal sector has the weakest diagnostic accuracy for glaucoma compared to other sectors (Chauhan et al. 2013). Development of automated algorithms to segment the RNFL only within the rim may be necessary and have clinical benefit if future studies were to demonstrate improved diagnostic accuracy of adjusted MRW measurements.

In summary, we demonstrated that most normal subjects had at least one MRW measurement point within radial ONH scans in which retinal layers in addition to the RNFL are included in the measurement of MRW. These PRL were measured as part of the MRW in almost 12% of the total number of measurement points. The clinical relevance of these findings and whether PRL have any impact on the diagnosis and follow-up of glaucoma remain to be determined.

Acknowledgments

Funding/Support: Dalhousie Medical Research Foundation, Halifax, NS, Canada (BCC), National Eye Institute, National Institutes of Health, Bethesda MD (grant no. EY021281, CFB), Center for Disease Control, Atlanta, GA (CAG), Heidelberg Engineering, Heidelberg, Germany (JC, SD, CAG, MH, AI, JML, CYM, TN, HAQ, AFS, KS, HT, GT, YY, CFB, BCC)

Financial disclosures: Commercial Relationships: Heidelberg Engineering, MA, JC, SD, CAG, MH, AI, JML, CYM, TN, HAQ, AFS, KS, HT, GT, YY, CFB, BCC (F)

References

Anderson DR, Hoyt WF. Ultrastructure of intraorbital portion of human and monkey optic nerve. Arch Ophthalmol (Chicago, Ill 1960). 1969; 82:506–30.

Chauhan BC, Burgoyne CF. From Clinical Examination of the Optic Disc to Clinical Assessment of the Optic Nerve Head: A Paradigm Change. Am J Ophthalmol. 2013; 156:218–227. [PubMed: 23768651]

Chauhan BC, Danthurebandara VM, Sharpe GP, Demirel S, Girkin CA, Mardin CY, Scheuerle AF, Burgoyne CF. Bruch's Membrane Opening Minimum Rim Width and Retinal Nerve Fiber Layer Thickness in a Normal White Population: A Multicenter Study. Ophthalmology. 2015; 122:1786–94. [PubMed: 26198806]

Chauhan BC, O'Leary N, Almobarak FA, et al. Enhanced detection of open-angle glaucoma with an anatomically accurate optical coherence tomography-derived neuroretinal rim parameter. Ophthalmology. 2013; 120:535–43. [PubMed: 23265804]

Chen TC. Spectral domain optical coherence tomography in glaucoma: qualitative and quantitative analysis of the optic nerve head and retinal nerve fiber layer (an AOS thesis). Trans Am Ophthalmol Soc. 2009; 107:254–81. [PubMed: 20126502]

Curcio CA, Allen KA. Topography of ganglion cells in human retina. J Comp Neurol. 1990; 300:5–25. [PubMed: 2229487]

Curcio CA, Sloan KR, Kalina RE, Hendrickson AE. Human photoreceptor topography. J Comp Neurol. 1990; 292:497–523. [PubMed: 2324310]

Danthurebandara VM, Sharpe GP, Hutchison DM, Denniss J, Nicolela MT, McKendrick AM, Turpin A, Chauhan BC. Enhanced structure-function relationship in glaucoma with an anatomically and geometrically accurate neuroretinal rim measurement. Invest Ophthalmol Vis Sci. 2014; 56:98–105. [PubMed: 25503459]

Fan N, Huang N, Lam DSC, Leung CK-S. Measurement of Photoreceptor Layer in Glaucoma: A Spectral-Domain Optical Coherence Tomography Study. J Ophthalmol. 2011; 2011:1–5.

Fortune B, Hardin C, Reynaud J, Cull G, Yang H, Wang L, Burgoyne CF. Comparing Optic Nerve Head Rim Width, Rim Area, and Peripapillary Retinal Nerve Fiber Layer Thickness to Axon Count in Experimental Glaucoma. Invest Ophthalmol Vis Sci. 2016; 57:OCT404–12. [PubMed: 27409499]

Gardiner SK, Ren R, Yang H, Fortune B, Burgoyne CF, Demirel S. A method to estimate the amount of neuroretinal rim tissue in glaucoma: Comparison with current methods for measuring rim area. Am J Ophthalmol. 2014; 157:957–970.

Garway-Heath DF, Poinoosawmy D, Fitzke FW, Hitchings RA. Mapping the visual field to the optic disc in normal tension glaucoma eyes. Ophthalmology. 2000; 107:1809–15. [PubMed: 11013178]

Girkin CA, McGwin G, Sinai MJ, et al. Variation in optic nerve and macular structure with age and race with spectral-domain optical coherence tomography. Ophthalmology. 2011; 118:2403–2408. [PubMed: 21907415]

Hasegawa T, Ooto S, Takayama K, et al. Cone Integrity in Glaucoma: An Adaptive-Optics Scanning Laser Ophthalmoscopy Study. Am J Ophthalmol. 2016; 171:53–66. [PubMed: 27565227]

Ishikawa H, Stein DM, Wollstein G, Beaton S, Fujimoto JG, Schuman JS. Macular segmentation with optical coherence tomography. Invest Ophthalmol Vis Sci. 2005; 46:2012–7. [PubMed: 15914617]

Kendell KR, Quigley HA, Kerrigan LA, Pease ME, Quigley EN. Primary open-angle glaucoma is not associated with photoreceptor loss. Invest Ophthalmol Vis Sci. 1995; 36:200–5. [PubMed: 7822147]

Knight OJ, Girkin CA, Budenz DL, Durbin MK, Feuer WJ, Cirrus OCT Normative Database Study Group. Effect of race, age, and axial length on optic nerve head parameters and retinal nerve fiber layer thickness measured by Cirrus HD-OCT. Arch Ophthalmol (Chicago, Ill 1960). 2012; 130:312–8.

Knighton RW, Gregori G, Budenz DL. Variance reduction in a dataset of normal macular ganglion cell plus inner plexiform layer thickness maps with application to glaucoma diagnosis. Invest Ophthalmol Vis Sci. 2012; 53:3653–61. [PubMed: 22562512]

Kotowski J, Folio LS, Wollstein G, Ishikawa H, Ling Y, Bilonick RA, Kagemann L, Schuman JS. Glaucoma discrimination of segmented cirrus spectral domain optical coherence tomography (SD-OCT) macular scans. Br J Ophthalmol. 2012; 96:1420–5. [PubMed: 22914498]

Landis JR, Koch GG. The measurement of observer agreement for categorical data. Biometrics. 1977; 33:159–74. [PubMed: 843571]

Lei Y, Garrahan N, Hermann B, Becker DL, Hernandez MR, Boulton ME, Morgan JE. Quantification of retinal transneuronal degeneration in human glaucoma: a novel multiphoton-DAPI approach. Invest Ophthalmol Vis Sci. 2008; 49:1940–5. [PubMed: 18436826]

Na JH, Sung KR, Baek S, Kim YJ, Durbin MK, Lee HJ, Kim HK, Sohn YH. Detection of glaucoma progression by assessment of segmented macular thickness data obtained using spectral domain optical coherence tomography. Invest Ophthalmol Vis Sci. 2012; 53:3817–26. [PubMed: 22562510]

Patel NB, Sullivan-Mee M, Harwerth RS. The relationship between retinal nerve fiber layer thickness and optic nerve head neuroretinal rim tissue in glaucoma. Invest Ophthalmol Vis Sci. 2014; 55:6802–16. [PubMed: 25249610]

Pollet-Villard F, Chiquet C, Romanet J-P, Noel C, Aptel F. Structure-function relationships with spectral-domain optical coherence tomography retinal nerve fiber layer and optic nerve head measurements. Invest Ophthalmol Vis Sci. 2014; 55:2953–62. [PubMed: 24692125]

Povazay B, Hofer B, Hermann B, Unterhuber A, Morgan JE, Glittenberg C, Binder S, Drexler W. Minimum distance mapping using three-dimensional optical coherence tomography for glaucoma diagnosis. J Biomed Opt. 2007; 12:41204.

Rao HL, Babu GJ, Sekhar GC. Comparison of the diagnostic capability of the Heidelberg Retina Tomographs 2 and 3 for glaucoma in the Indian population. Ophthalmology. 2010; 117:275–81. [PubMed: 19969365]

Reis ASC, O'Leary N, Yang H, Sharpe GP, Nicolela MT, Burgoyne CF, Chauhan BC. Influence of clinically invisible, but optical coherence tomography detected, optic disc margin anatomy on neuroretinal rim evaluation. Invest Ophthalmol Vis Sci. 2012; 53:1852–1860. [PubMed: 22410561]

Reis ASC, Sharpe GP, Yang H, Nicolela MT, Burgoyne CF, Chauhan BC. Optic disc margin anatomy in patients with glaucoma and normal controls with spectral domain optical coherence tomography. Ophthalmology. 2012; 119:738–47. [PubMed: 22222150]

Rhodes LA, Huisingh C, Johnstone J, et al. Variation of laminar depth in normal eyes with age and race. Invest Ophthalmol Vis Sci. 2014; 55:8123–33. [PubMed: 25414182]

Rhodes LA, Huisingh C, Johnstone J, et al. Peripapillary choroidal thickness variation with age and race in normal eyes. Invest Ophthalmol Vis Sci. 2015; 56:1872–9. [PubMed: 25711640]

Rhodes LA, Huisingh CE, Quinn AE, McGwin G, LaRussa F, Box D, Owsley C, Girkin CA. Comparison of Bruch's Membrane Opening Minimum Rim Width Among Those With Normal Ocular Health by Race. Am J Ophthalmol. 2017; 174:113–118. [PubMed: 27825982]

Springer AD, Hendrickson AE. Development of the primate area of high acuity. 1. Use of finite element analysis models to identify mechanical variables affecting pit formation. Vis Neurosci. 2004; 21:53–62. [PubMed: 15137581]

Springer AD, Hendrickson AE. Development of the primate area of high acuity. 2. Quantitative morphological changes associated with retinal and pars plana growth. Vis Neurosci. 2004; 21:775–90. [PubMed: 15683563]

Springer AD, Hendrickson AE. Development of the primate area of high acuity, 3: temporal relationships between pit formation, retinal elongation and cone packing. Vis Neurosci. 2005; 22:171–85. [PubMed: 15935110]

Strouthidis NG, Fortune B, Yang H, Sigal IA, Burgoyne CF. Longitudinal change detected by spectral domain optical coherence tomography in the optic nerve head and peripapillary retina in experimental glaucoma. Invest Ophthalmol Vis Sci. 2011; 52:1206–19. [PubMed: 21217108]

Strouthidis NG, Yang H, Downs JC, Burgoyne CF. Comparison of clinical and three-dimensional histomorphometric optic disc margin anatomy. Invest Ophthalmol Vis Sci. 2009; 50:2165–74. [PubMed: 19136694]

Strouthidis NG, Yang H, Reynaud JF, Grimm JL, Gardiner SK, Fortune B, Burgoyne CF. Comparison of clinical and spectral domain optical coherence tomography optic disc margin anatomy. Invest Ophthalmol Vis Sci. 2009; 50:4709–18. [PubMed: 19443718]

Tan O, Li G, Lu AT-H, Varma R, Huang D, Advanced Imaging for Glaucoma Study Group. Mapping of macular substructures with optical coherence tomography for glaucoma diagnosis. Ophthalmology. 2008; 115:949–56. [PubMed: 17981334]

Varela HJ, Hernandez MR. Astrocyte responses in human optic nerve head with primary open-angle glaucoma. J Glaucoma. 1997; 6:303–13. [PubMed: 9327349]

Vianna JR, Malik R, Danthurebandara VM, Sharpe GP, Belliveau AC, Shuba LM, Chauhan BC, Nicolela MT. Beta and Gamma Peripapillary Atrophy in Myopic Eyes With and Without Glaucoma. Invest Ophthalmol Vis Sci. 2016; 57:3103–11. [PubMed: 27294804]

Wang L, Cioffi GA, Cull G, Dong J, Fortune B. Immunohistologic evidence for retinal glial cell changes in human glaucoma. Invest Ophthalmol Vis Sci. 2002; 43:1088–94. [PubMed: 11923250]

Werner JS, Keltner JL, Zawadzki RJ, Choi SS. Outer retinal abnormalities associated with inner retinal pathology in nonglaucomatous and glaucomatous optic neuropathies. Eye (Lond). 2011; 25:279–89. [PubMed: 21293495]

Wilsey LJ, Reynaud J, Cull G, Burgoyne CF, Fortune B. Macular Structure and Function in Nonhuman Primate Experimental Glaucoma. Invest Ophthalmol Vis Sci. 2016; 57:1892–900. [PubMed: 27082305]

Wygnanski T, Desatnik H, Quigley HA, Glovinsky Y. Comparison of ganglion cell loss and cone loss in experimental glaucoma. Am J Ophthalmol. 1995; 120:184–9. [PubMed: 7639302]

Yang H, Ren R, Lockwood H, Williams G, Libertiaux V, Downs C, Gardiner SK, Burgoyne CF. The Connective Tissue Components of Optic Nerve Head Cupping in Monkey Experimental Glaucoma Part 1: Global Change. Invest Ophthalmol Vis Sci. 2015; 56:7661–78. [PubMed: 26641545]

Yang H, Reynaud J, Lockwood H, et al. The connective tissue phenotype of glaucomatous cupping in the monkey eye - Clinical and research implications. Prog Retin Eye Res. 2017; 59:1–52. [PubMed: 28300644]

Yang H, Thompson H, Roberts MD, Sigal IA, Downs JC, Burgoyne CF. Deformation of the early glaucomatous monkey optic nerve head connective tissue after acute IOP elevation in 3-D histomorphometric reconstructions. Invest Ophthalmol Vis Sci. 2011; 52:345–63. [PubMed: 20702834]

Ye C, Yu M, Leung CK-S. Impact of segmentation errors and retinal blood vessels on retinal nerve fibre layer measurements using spectral-domain optical coherence tomography. Acta Ophthalmol. 2016; 94:e211–9. [PubMed: 26132774]

Zelefsky JR, Harizman N, Mora R, Ilitchev E, Tello C, Ritch R, Liebmann JM. Assessment of a race-specific normative HRT-III database to differentiate glaucomatous from normal eyes. J Glaucoma. 2006; 15:548–51. [PubMed: 17106370]

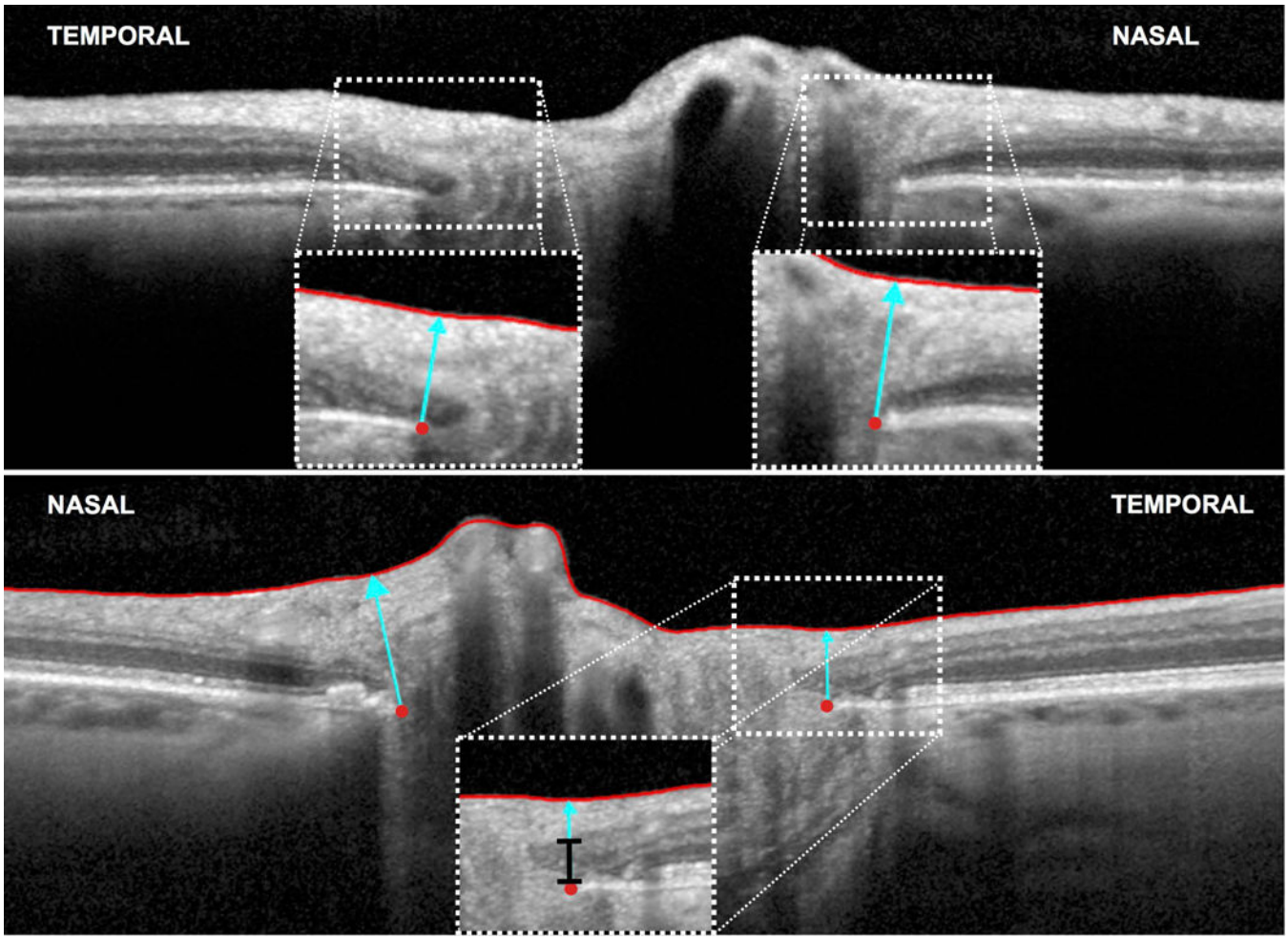

Figure 1.

Protruded retinal layers (PRL) in the neuroretinal rim in two radial B-scans (top and bottom) obtained with optical coherence tomography of the optic nerve head and peripapillary retina. In both images, PRL were present at the temporal measurement point but absent at the nasal point (insets). Bottom image shows PRL thickness (black bar with caps) as a proportion of the minimum rim width (MRW, blue arrow, inset). In this case, the PRL thickness (102 μm) corresponds to 44% of the measured MRW. Red lines show the internal limiting membrane and red dots show Bruch's membrane opening.

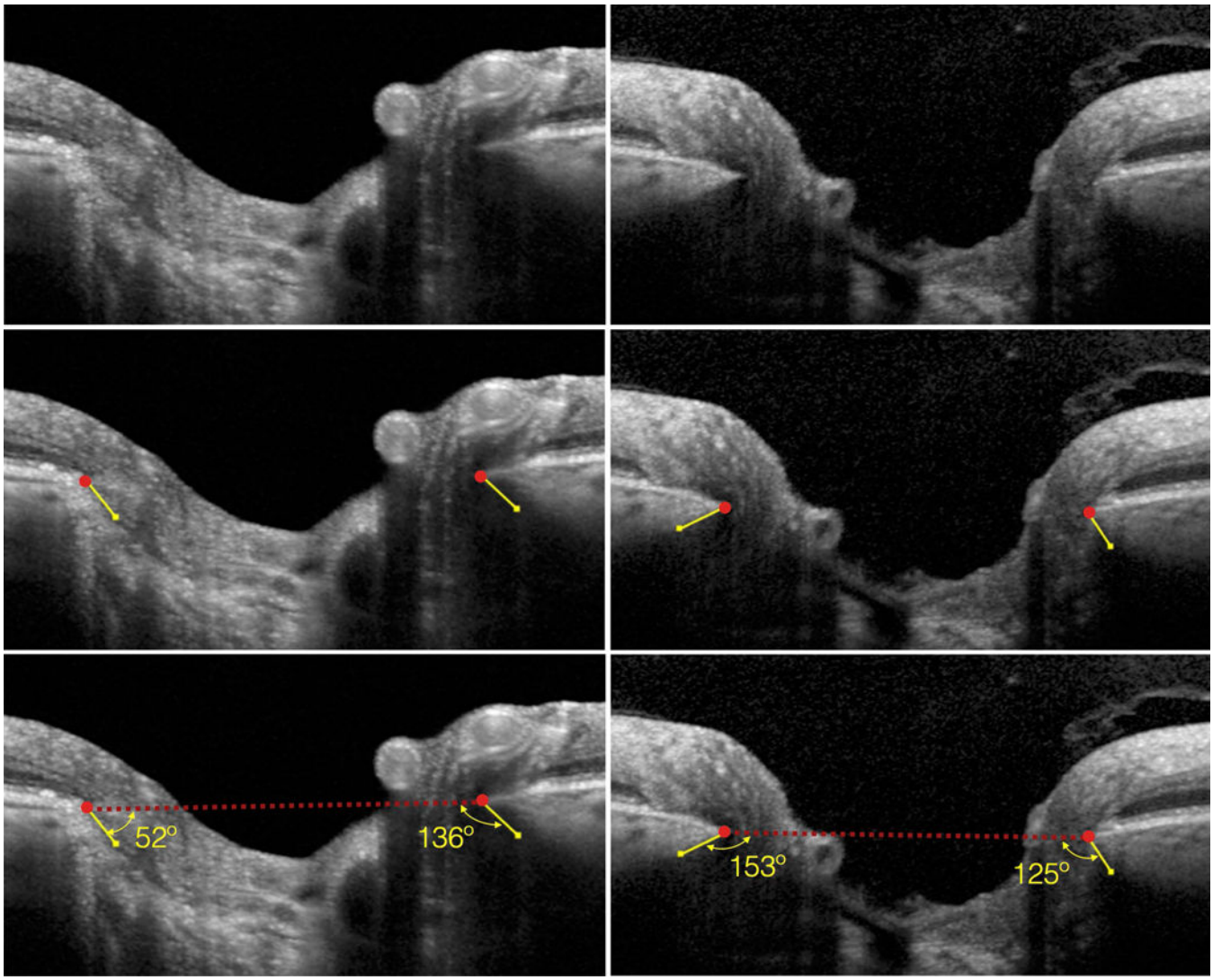

Figure 2.

Border tissue angle segmentation in B-scans of two optic nerve head radial B-scans subjects (left and right images, respectively). Top images: unmarked images. Middle images: from each Bruch's membrane opening (BMO) point (red dots), the border tissue is traced with a straight line (yellow line). Bottom images: the border tissue angle at each measurement point is calculated with relative to the BMO reference plane (red dotted line). The B-scan of one subject (left images) has one point with an externally oblique angle (52°) and another with an internally oblique angle (136°). The other subject (right images) has internally oblique angles at both measurement points (153° and 125°).

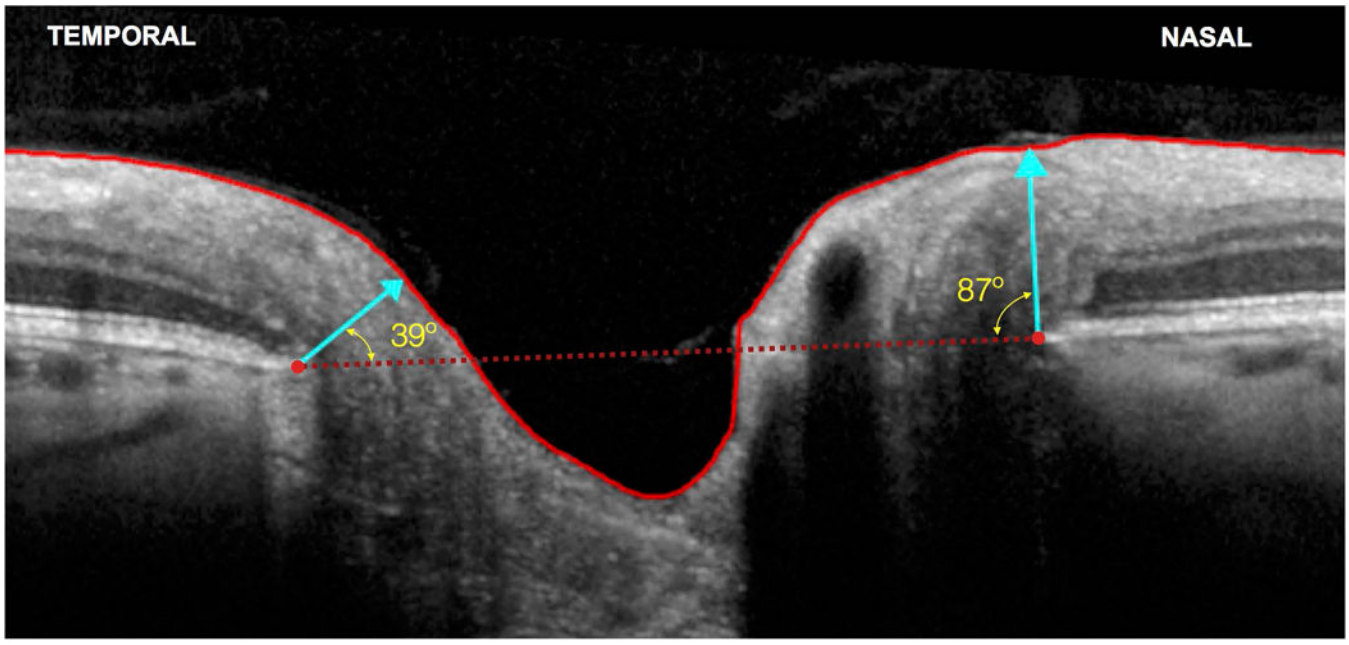

Figure 3.
Minimum rim width (MRW) vector orientation in each of the 2 measurement points in a B-scan. The MRW angles are measured from the Bruch's membrane opening (red dots) reference plane (dotted red line).

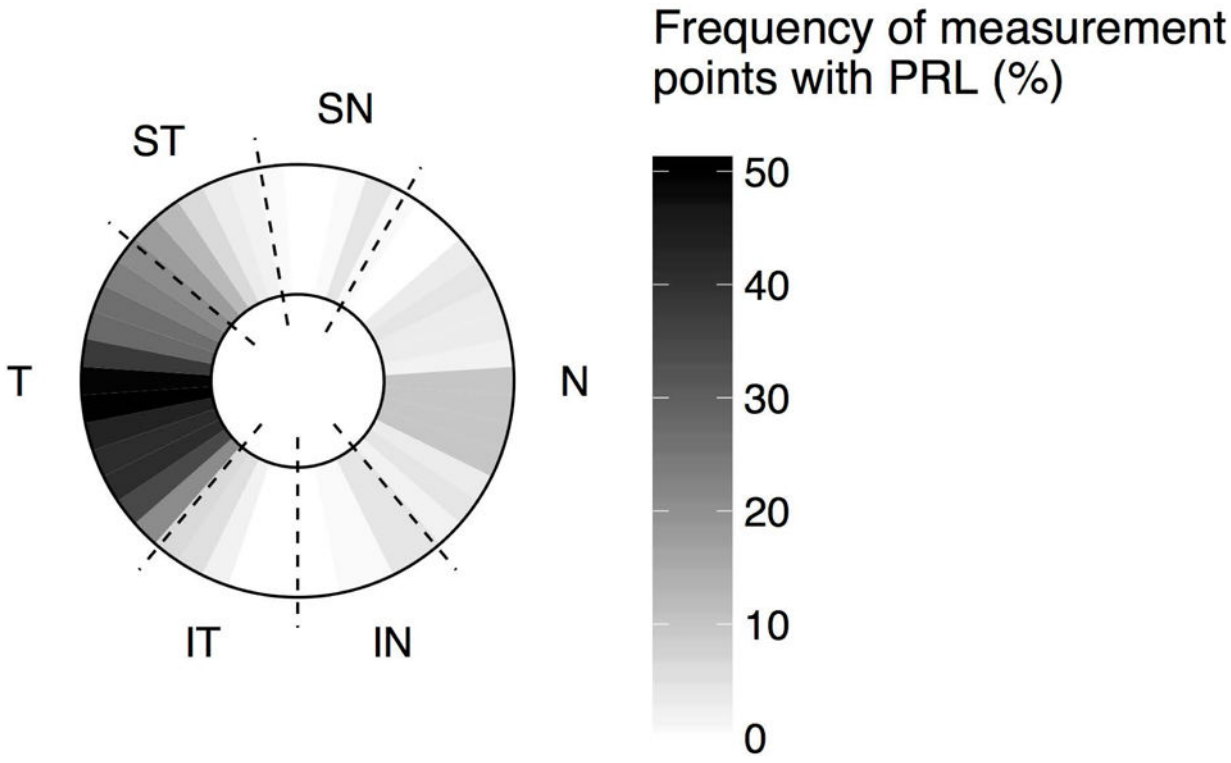

Figure 4.

Polar plot (in right eye format) showing the frequency of protruded retinal layers (PRL) in each of the 48 optic nerve head neuroretinal rim measurement points evaluated. The black dotted lines separate the 6 sectors. T = Temporal, ST = supero-temporal, SN = supero-nasal, N = nasal, IN = infero-nasal, IT = infero-temporal.

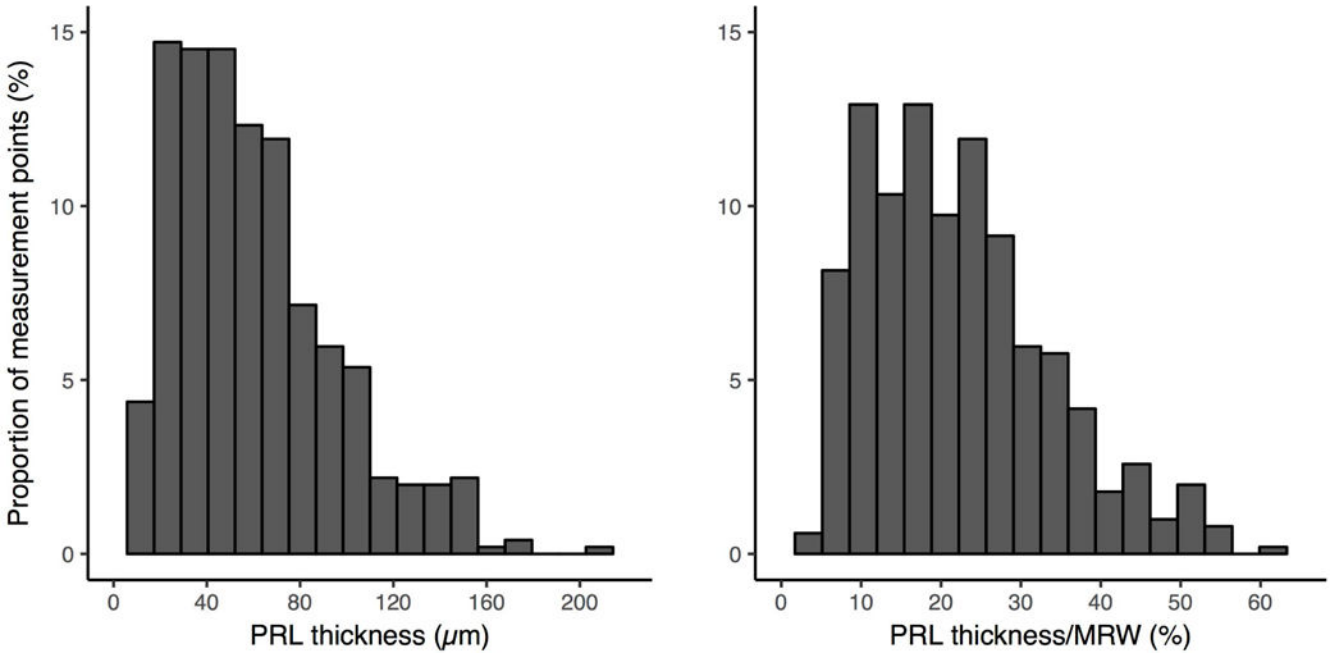

Figure 5.

Histograms showing the distribution of protruded retinal layers (PRL) thickness (left plot) and PRL thickness relative to the unadjusted minimum rim width (MRW, right plot) in those measurement points where PRL were present. The median values of PRL thickness and PRL thickness relative to the unadjusted MRW are 53.0 μm and 20.6%, respectively.

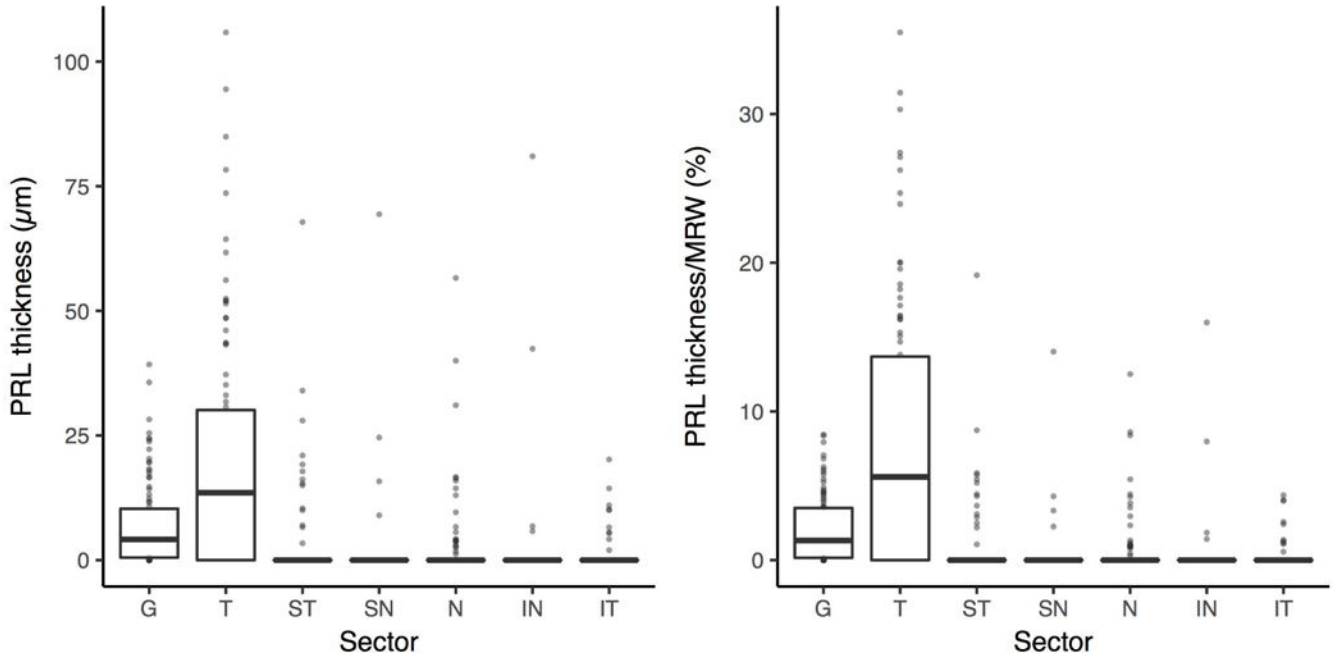

Figure 6.

Box plots showing the global and sectoral distribution of the protruded retinal layers (PRL) thickness (left plot) and the PRL thickness proportion relative to the MRW (computed PRL thickness/unadjusted MRW, right plot). The data points above or below the box plots represent values outside the interquartile range. MRW = minimum rim width, G = global, T = temporal, ST = supero-temporal, SN = supero-nasal, N = nasal, IN = infero-nasal, IT = infero-temporal.

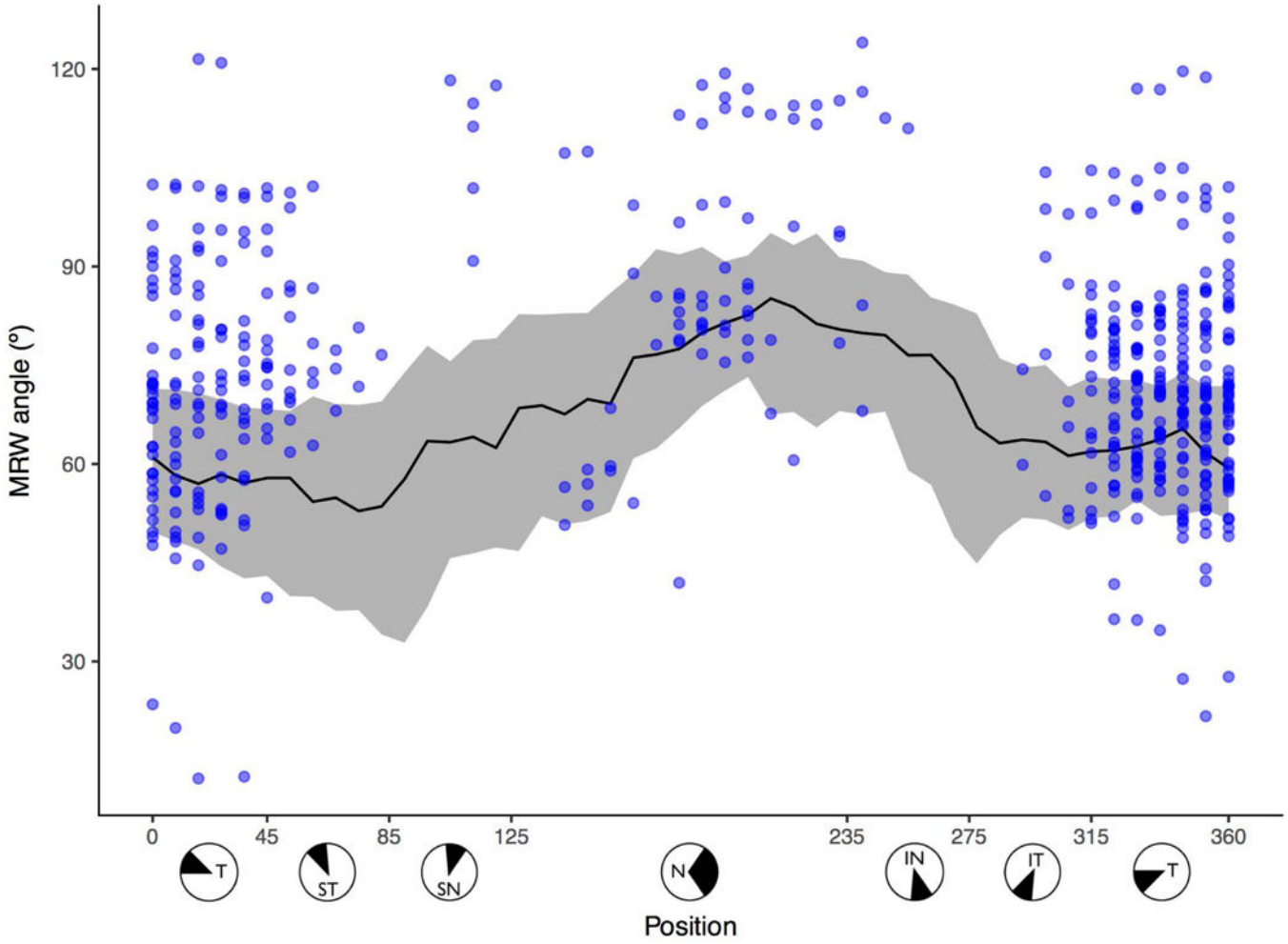

Figure 7.

Minimum rim width (MRW) angle distribution. Median and interquartile ranges of all measurement points in all subjects are represented by bold lines and gray shading, respectively. MRW angle in points with protruded retinal layers (PRL, blue dots). A median of 66.7 (interquartile range: 49.5 to 100.0)% of the blue dots were above the bold line, indicating that the MRW angles for the points with PRL are generally greater than the MRW angles in all points. T = temporal, ST = supero-temporal, SN = supero-nasal, N = nasal, IN = infero-nasal, IT = infero-temporal.

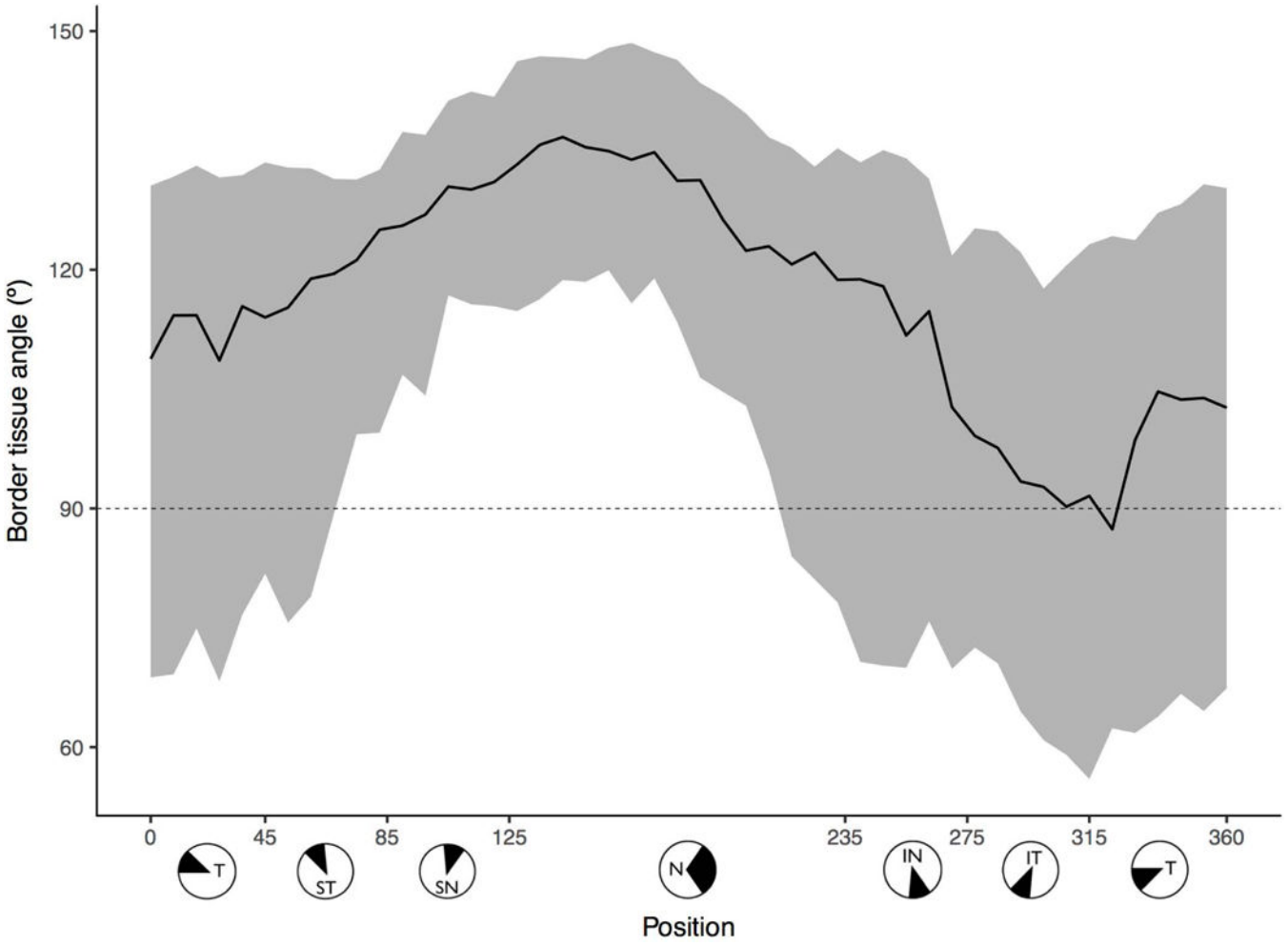

Figure 8.

Border tissue angle distribution in the optic nerve head. Median and interquartile ranges are represented by the bold line and gray shading, respectively. The dashed horizontal line separates border tissue angles corresponding to internally oblique configuration (> 90°) and externally oblique configuration (< 90°). T = temporal, ST = supero-temporal, SN = supero-nasal, N = nasal, IN = infero-nasal, IT = infero-temporal.

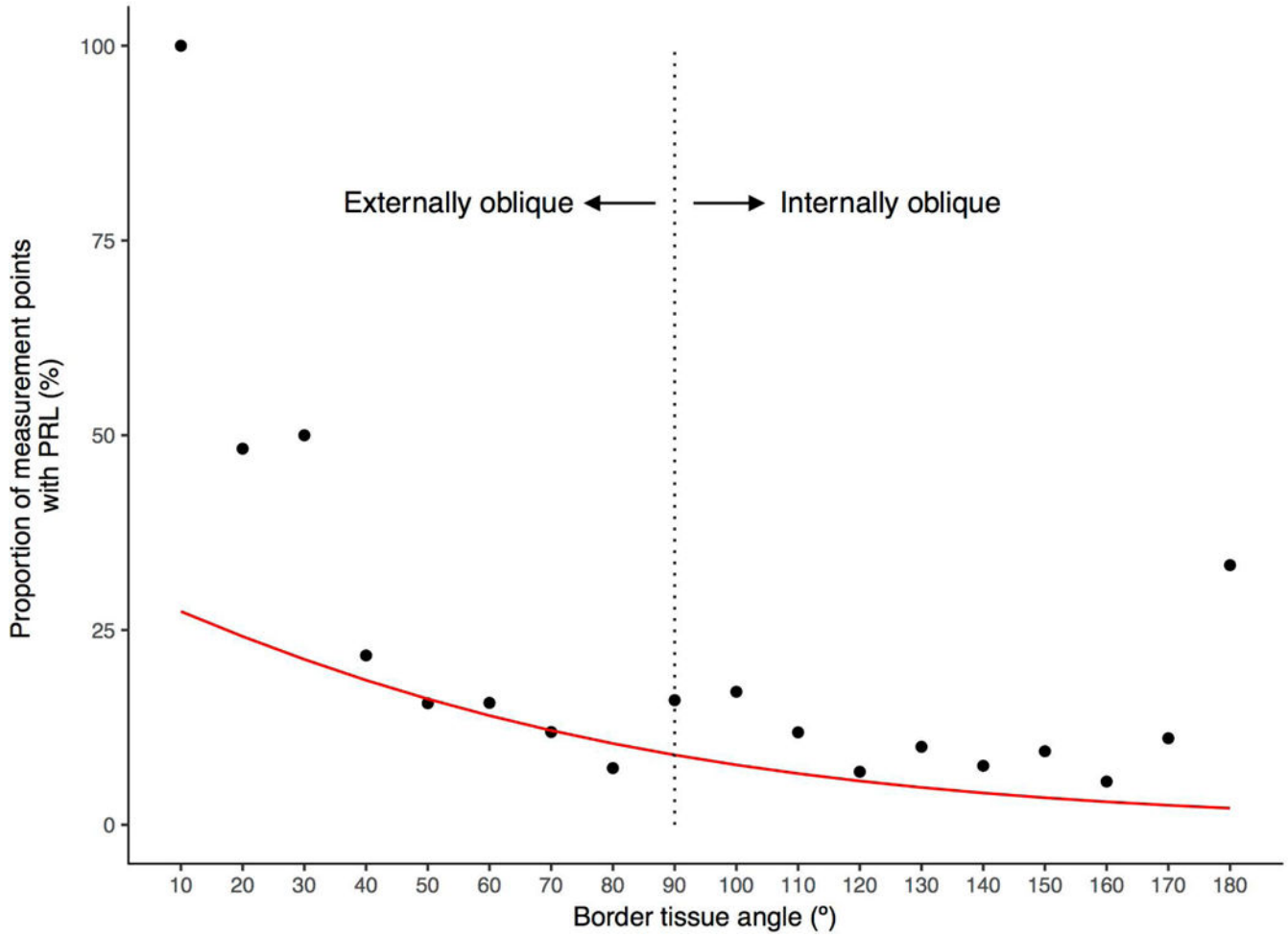

Figure 9.

Scatterplot showing the influence of each 10° change in border tissue angle on the frequency of protruded retinal layers (PRL). The red line, generated by a logistic mixed effect model, represents the predicted relationship. The dashed vertical line separates border tissue angles corresponding to internally oblique configuration (> 90°) and externally oblique configuration (< 90°).

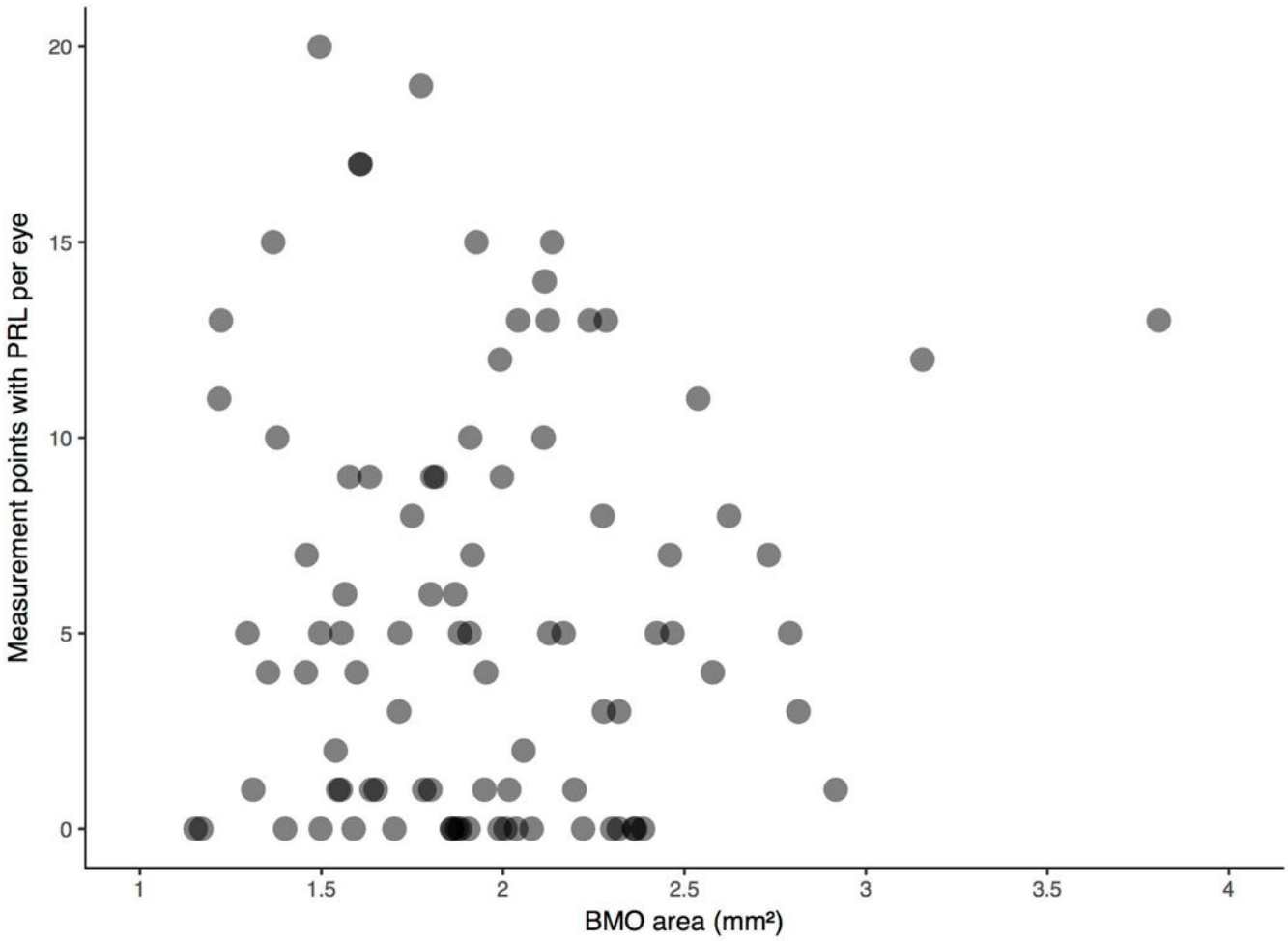

Figure 10.

Scatterplot showing the association between Bruch's membrane opening (BMO) area and the number of measurement points with protruded retinal layers (PRL).

Table 1

Summary of subject characteristics*

	All	White	Black	Japanese	*P*
Age (years)	49.5 (36.6 to 63.5)	49.5 (36.6 to 62.6)	49.3 (36.6 to 63.5)	49.9 (35.3 to 64.2)	0.42
Refraction (D)	0.0 (−1.2 to 0.6)	0.1 (−0.5 to 0.6)	−0.6 (−1.5 to 0.0)	−0.1 (−1.0 to 1.1)	<0.01
BMO area (mm^1)	1.9 (1.6 to 2.2)	1.9 (1.5 to 2.1)	1.8 (1.5 to 2.1)	2.1 (1.9 to 2.4)	<0.01
Global unadjusted MRW (μm)	320.0 (282.3 to 356.5)	337.4 (302.1 to 382.9)	325.1 (300.6 to 356.5)	288.6 (262.1 to 329.2)	<0.01
Global adjusted MRW (μm)	310.7 (276.4 – 350.5)	330.0 (287.1 – 365.8)	317.1 (291.7 – 355.6)	287.6 (261.8 – 328.8)	<0.01

* Median and interquartile range

BMO = Bruch's membrane opening

MRW = Minimum rim width

Table 2

Frequency of protruded retinal layers

	All	White	Black	Japanese	*P*
Subjects with PRL	69 (76.6%)	29 (96.6%)	22 (73.3%)	18 (60.0%)	<0.01
Total number of positions with PRL	503 (11.6%)	218 (15.1%)	181 (12.6%)	104 (7.2%)	<0.01
Percentage of positions with PRL per subject *	10.4% (2.1 to 18.8%)	12.5% (8.3 to 23.0%)	10.4% (0.5 to 18.8%)	2.1% (2.1 to 10.4%)	<0.01

* Median and interquartile range

PRL = protruded retinal layers